Au nanoparticles/hollow molybdenum disulfide microcubes based biosensor for microRNA-21 detection coupled with duplex-specific nuclease and enzyme signal amplification

Hong-Lei Shuai, Ke-Jing Huang, Ying-Xu Chen, Lin-Xia Fang, Meng-Pei Jia

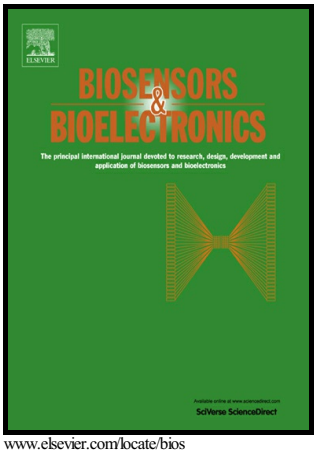

www.elsevier.com/locate/bios

PII: S0956-5663(16)31056-9
DOI: http://dx.doi.org/10.1016/j.bios.2016.10.051
Reference: BIOS9273

To appear in: *Biosensors and Bioelectronic*

Received date: 3 July 2016
Revised date: 30 September 2016
Accepted date: 18 October 2016

Cite this article as: Hong-Lei Shuai, Ke-Jing Huang, Ying-Xu Chen, Lin-Xia Fang and Meng-Pei Jia, Au nanoparticles/hollow molybdenum disulfide microcubes based biosensor for microRNA-21 detection coupled with duplex specific nuclease and enzyme signal amplification, *Biosensors and Bioelectronic* http://dx.doi.org/10.1016/j.bios.2016.10.051

Au nanoparticles/hollow molybdenum disulfide microcubes based biosensor for microRNA-21 detection coupled with duplex-specific nuclease and enzyme signal amplification

Hong-Lei Shuai [a], Ke-Jing Huang [a,b,*], Ying-Xu Chen [a], Lin-Xia Fang [a], Meng-Pei Jia [a]

[a] College of Chemistry and Chemical Engineering, Xinyang Normal University, Xinyang 464000, China

[b] Institute for Conservation and Utilization of Agro-bioresources in Dabie Mountains, Xinyang Normal University, Xinyang 464000, China

[*]Corresponding author. Tel.: +86-376-6390611

E-mail address: kejinghuang11@163.com (K.J. Huang)

Abstract

An ultrasensitive electrochemical biosensor for detecting microRNAs is fabricated based on hollow molybdenum disulfide (MoS_2) microcubes. Duplex-specific nuclease, enzyme and electrochemical–chemical–chemical redox cycling are used for signal amplification. Hollow MoS_2 microcubes constructed by ultrathin nanosheets are synthesized by a facile template-assisted strategy and used as supporting substrate. For biosensor assembling, biotinylated ssDNA capture probes are first immobilized on Au nanoparticles (AuNPs)/MoS_2 modified electrode in order to combine with streptavidin-conjugated alkaline phosphatase (SA-ALP). When capture probes hybridize with miRNAs, duplex-specific nuclease cleaves the formative duplexes. At the moment, the biotin group strips from the electrode surface and SA-ALP is incapacitated to attach onto electrode. Then, ascorbic acids induce the electrochemical–chemical–chemical redox cycling to produce electrochemical response in the presence of ferrocene methanol and tris (2-carboxyethyl) phosphine. Under optimum conditions, the proposed biosensor shows a good linear relationship between the current variation and logarithm of the microRNAs concentration ranging from 0.1 fM to 0.1 pM with a detection limit of 0.086 fM (S/N=3). Furthermore, the biosensor is successfully applied to detect target miRNA-21 in human serum samples.

Keywords: Hollow molybdenum disulfide microcubes; Duplex-specific nuclease; MicroRNAs; Enzyme signal amplification; Electrochemical biosensor

1. Introduction

MicroRNAs (miRNAs) are a class of small non-coding RNA molecules that play critical functions in many biological processes, such as developmental regulation, proliferation, differentiation, cardiogenesis, and epigenetic inheritance (Li et al., 2015; Xia et al., 2015). Recently, accumulative evidences indicate that miRNAs are highly correlated to the cancer initiation, oncogenesis and tumor response to treatments (Ge et al., 2014; Bi et al., 2015). The presence of miRNAs in serum has been accurately detected and they have been regarded as clinically important biomarkers for early cancer diagnostic, drug discovery targets and prognostic processes (Hong et al., 2013; Yang et al., 2012; Dong et al., 2013). In the past year, traditional biological methods for miRNA detection have been developed including northern blotting, microarray and quantitative reverse transcription polymerase chain reaction (Hunt et al., 2015). Most recently, electrochemical assays have gotten wide attention in miRNA analysis due to their simplicity, sensitivity and rapidity (Leshkowitz et al., 2013; Miao et al., 2015). However, it still remains significant challenges in the ultrasensitive and specific aspects due to the low abundance of miRNAs in biological samples (Liu et al., 2015; Miao et al., 2015).

Two-dimensional (2D) nanomaterial has been proved a key factor in the fabrication of electrochemical biosensor due to large specific surface area and usual good electro-conductivity (Guo et al., 2013). Most recently, layered transition-metal dichalcogenides attract increasing attention due to their unique properties (Huang et al., 2014a; Huang et al., 2014b; Liu et al., 2015; Wang et al., 2015a; Luo and Liu, 2015). As a typical member, molybdenum disulfide (MoS_2) can be isolated as monolayer or few-layer thick sheets. It is composed of Mo metal layers sandwiched between two sulfur layers and stacked together by weak Van der Waals interactions,

and has aroused increasing academic interest due to unique optical, electronic and catalytic properties (Ou et al., 2014; Gao et al., 2015). The most noteworthy is MoS_2 nanosheets can spontaneously adsorb single-stranded DNA but hardly interact with rigid double-stranded DNA (Zhu et al., 2013). Whereas, because of the high surface energy and interlayer Van der Waals attraction, restacking of MoS_2 nanosheets is almost unescapable in practical applications, which greatly reduces the effective specific surface area, and therefore weakens its performance in some degree (Chhowalla et al., 2013; Hwang et al., 2011). So, assembling primordial 2D nanosheets into three-dimensional architectures is very significative.

Herein, hollow MoS_2 microcubes are prepared by a facile template-assisted approach. An ultrasensitive electrochemical sensor for detecting miRNA-21 is fabricated based on hollow MoS_2 microcubes coupling with duplex-specific nuclease (DSN), enzyme signal amplification and electrochemical–chemical–chemical (EEC) redox cycling. EEC redox cycling has been proved as an effective signal-amplification technique (Wang, et al., 2011; Yang, 2012). DSN is an enzyme that exhibits a great preference for cleaving double-stranded DNA or DNA in DNA/RNA hybrid duplexes, and is not only practically inactive toward single stranded DNA, or single or double-stranded RNA but also shows a eminent capability to distinguish whether perfectly matched short duplexes or not (Xi et al., 2014). In addition, capture probes hybridized with miRNAs can be cleaved by DSN, and miRNAs are released and recycled in sample solution (Degliangeli et al., 2014). ECC redox cycling uses ferrocene methanol (FcM) as redox mediator. Redox cycling electrons are transferred between redox mediators and enzymatic products. Furthermore, enzymatic product of alkaline phosphatase (ALP) can be regenerated immediately by extra chemical reducing reagent after their oxidation. Therefore, this proposed method is more

sensitive than that obtained by single or multiplex enzyme amplification. In this work, MoS_2 microcubes with large specific surface couple with AuNPs to act as an excellent sensing substrate, which can immobilize large amount of capture DNA and in turn lead to a low detection limit. DSN can cleave the DNA-miRNAs duplexes and miRNAs strands can recycle in the sample solution. The application of enzyme and EEC redox cycling can greatly amplify detection signal. Combination of three above advangtages empowers proposed assay ultrahigh sensitivity and excellent selectivity for target miRNA detection.

2. Experimental

2.1. Reagents and materials

$MnSO_4 \cdot H_2O$, sodium molybdate and $HAuCl_4 \cdot 3H_2O$ were obtained from Aladdin Chemicals Co. Ltd. (Shanghai, China). Diethylpyrocarbonate, tris(carboxyethyl)phosphine (TCEP), 6-mercaptohexanol (MCH), streptavidin-conjugated alkaline phosphatase (SA-ALP), bovine serum albumin (BSA) and tris-(hydroxymethyl)aminomethane hydrochloride (Tris–HCl) were purchased from Sigma-Aldrich (Shanghai, China). Duplex-specific nuclease was supplied by Evrogen Joint Stock Company (Moscow, Russia). MiRNAs and DNA sequences were synthesized by Shanghai Sangon Biological Engineering Technology Co. Ltd. (Shanghai, China) and their sequences were as follows:

Capture probe: 5'-biotin-TCAACATCAGTCTGATAAGCTATTT-$(CH_2)_6$-SH-3'

MiRNA-21: 5'-UAGCUUAUCAGACUGAUGUUGA-3'

Single-base mismatch: 5'-UAGCUUAUCGGACUGAUGUUGA-3'

Three-base mismatch: 5'-UUGCUUAUCGGACUGAUCUUGA-3'

Non-complementary: 5'-GUAAGGCAUCUGACCGAAGGCA-3'

DNA solutions were prepared in TE buffer solution (10 mM Tris–HCl, 1 mM EDTA, pH 7.4). The stock solution of FcM and TCEP were prepared in Tris buffer solution (10 mM, pH 8.0).

2.2. Apparatus

All electrochemical measurements were performed on an EC550 electrochemical workstation (Wuhan, Gaoss Union, China) with a conventional three-electrode system composed of a platinum wire as an auxiliary electrode, a saturated calomel electrode (SCE) as reference electrode and a 3-mm diameter glassy carbon electrode (GCE) as working electrode. Nanostructures were characterized by a JEM 2100 transmission electron microscope (TEM, JEOL, Tokyo, Japan) and a Hitachi S-4800 scanning electron microscope (SEM, Tokyo, Japan). X-ray diffraction (XRD) pattern was operated on a model D/max-rA diffractometer (Rigaku, Japan). Raman spectra were recorded at ambient temperature on a Renishaw Raman system model 1000 spectrometer (Gloucestershire, UK).

2.3. Preparation of hollow MoS_2 microcubes

$MnCO_3$ microcubes were synthesized according to a previous protocol (Fei et al., 2008). Firstly, 100 mmol $(NH_4)_2SO_4$, 10 mmol $MnSO_4 \cdot H_2O$ and 70 mL ethanol were dispersed in 700 mL water to obtain solution A. 100 mmol NH_4HCO_3 was dispersed in 700 mL water to obtain solution B. Then, solution B was added into solution A under vigorous stirring. Finally, the mixed solution was heated at 50 °C for 9 h. The white $MnCO_3$ precipitate was collected by centrifugation, washed thoroughly with water, and dried at 60 °C.

To grow MoS_2 shell on $MnCO_3$ microcubes, 0.4 g $MnCO_3$ microcubes were first dispersed in 40 mL water by ultrasonication for 60 min. 0.6 g sodium molybdate was added to above solution and mixed. Then, 2.5 g L-cysteine was added and stirred for another 10 min. Finally, the mixture was transferred to an 80-mL Teflon-lined stainless steel autoclave and heated at 180 °C for 24 h. The black precipitate of MnS@MoS_2 core-shell microcubes was collected by centrifugation, washed thoroughly with ethanol, and dried at 60 °C for 12 h.

For synthesis of hollow MoS_2 microcubes, 50 mg MnS@MoS_2 core-shell microcubes were dispersed in 40 mL 1.0 M HCl for 24 h to remove MnS cores. The black product of hollow MoS_2 microboxes was rinsed with water and then dried at 60 °C.

2.4. Preparation of DNA biosensor and electrochemical measurements

1.0 mg hollow MoS_2 microcubes were dispersed in 1 mL water by uitrasonication for 20 min to get homogenous suspension (1 mg mL^{-1}). Bare GCE was polished sequentially with 0.3 and 0.05 μm alumina slurries, washed ultrasonically with water and ethanol and then dried with nitrogen gas. 6 μL hollow MoS_2 microcubes suspension was then applied on the cleaned GCE and dried in air. For assembling DNA capture probe, Au nanoparticles (AuNPs) were electrodeposited on MoS_2/GCE from a PBS (pH 7.0) solution containing 0.1% $HAuCl_4$ at a constant potential of −0.2 V for 40 s. After that, 8 μL 1 nM DNA capture probe solution (cDNA) was dropped on AuNPs/MoS_2/GCE and allowed to react overnight. After thoroughly washed with water to remove unbound DNA capture probe, 8 μL 1mM MCH and 1% BSA were dropped on cDNA/AuNPs/MoS_2/GCE for 30 min to block unreacted gold surface and eliminate nonspecific adsorption. Again, the electrode was

rinsed with water. 6 μL 1 nM miRNA-21 and 2 μL 0.01U DSN were applied on electrode and incubated at 65 °C for 1h. Then the electrode was rinsed with water. 6 μL 0.1 mg mL^{-1} SA-ALP was then dropped on the electrode and incubated for 40 min. Thereafter, the resulting electrode was incubated in 5 mL Tris buffer solution (10 mM, pH 8.0) containing 0.5 mM AAP and 1 mM $MgCl_2$ for 30 min. The resulting electrode was rinsed with water and used for electrochemical measurements.

For targets sensing, cyclic voltammetry (CV) was carried out in 0.1 M PBS (pH 7.0) containing 10 mmol L^{-1} $[Fe(CN)_6]^{3-/4-}$ and 0.1 mol L^{-1} KCl solution between a potential window of −0.2 V and 0.6 V with a scan rate of 100 mVs^{-1}. EIS measurements were performed in 0.1 M PBS (pH 7.0) containing 5.0 mmol L^{-1} $[Fe(CN)_6]^{3-/4-}$ and 0.1 mol L^{-1} KCl solution from 100 KHz to 0.1 Hz. DPV measurements were conducted in Tris buffer solution containing 5 mM TCEP and 2 mM FcM using a pulse amplitude of 50 mV, pulse width of 50 ms and pulse period of 0.2 s.

3. Results and discussion

3.1. Design principle of miRNA biosensor

The principle of miRNA biosensor fabrication is illustrated in Scheme 1. First, the designed thiolated DNA capture probe sequence which is complementary with miRNA is immobilized on AuNPs/MoS_2/GCE to form an upright probe through Au-S bond. Then, MCH and BSA are dropped on electrode to block unreacted gold surface and eliminate nonspecific adsorption. The biotin tags at the end of capture probe allow for the coupling of SA-ALP through streptavidin–biotin interaction, which will accelerate AA triggering ECC redox cycling. In detection system, FcM, TCEP and ascorbic acid 2-phosphate (AAP) are used as the redox mediator, reducing reagent and

enzyme substrate, respectively. Ferrocene derivatives have been reported to use as the mediators and are able to regenerate after its electrochemical oxidation with AA during the electrochemical scanning (Zhang et al., 2014). TCEP is a stable and electrochemically inert reducing regent showing no reaction with the oxidized form of ferrocene, which can regenerate AA from dehydroascorbic acid (DAA, the oxidation form of AA) (Akanda et al., 2011), thus enhancing the electrochemical signal. In these processes, SA-ALP is captured by electrode and used to catalyze the production of large amounts of AA, triggering ECC redox cycling. If capture probes hybridize with miRNAs, DSN cleaves the formative duplexes. At the moment, the biotin group strips from electrode and SA-ALP will be incapacitated to attach onto the electrode. Moreover, miRNAs strands can recycle in the sample solution due to be released and maintained integrity. The oxidation current of detection system decreases prominently with the increase of miRNA concentration. Since one miRNA molecule can induce the cleavage of thousands of capture probe strands during the hybridization/DSN incubation and initiate a plurality of redox reactions in the ECC recycling, the signal will decrease significantly, leading to a low detection limit.

3.2. Characterization of as-prepared materials

The morphology of $MnCO_3$, $MnS@MoS_2$ and MoS_2 microcubes were characterized with SEM and TEM. The SEM images of $MnCO_3$ microcubes are shown in Fig. 1A and B. It is clear $MnCO_3$ microcubes are uniform with a size of about 2 μm, which can well play the role of template to prop MoS_2 shell. Fig. 1C and D show typical SEM images of $MnS@MoS_2$. It manifests MnS microcubes are evenly covered with MoS_2 shell, and the size of these $MnS@MoS_2$ microcubes is about 2.5 μm. Some ruptured $MnS@MoS_2$ microcubes (Fig. 1D) distinctly display the shell is composed

with MoS_2 nanosheets. As shown in Figs. 1E and 1F, the 3D nanostructure (Fig. 1E) is faultlessly retained after removing MnS template. The SEM images of some ruptured MoS_2 microcubes (Fig. 1F) distinctly exhibit the hollow interior, and the thickness of the MoS_2 shell is about 400 nm. Fig. 1G shows the SEM images of BSA/MCH/Capture DNA/AuNPs/MoS_2/GCE after reacted with miRNA/DSN. It is obvious MoS_2 nanosheets covered with layers of modifiers. Figs. 1H–M show typical TEM images of $MnCO_3$, MnS@MoS_2 and MoS_2 microcubes, corresponding to above SEM images. As shown in Fig. 1H, $MnCO_3$ microcubes are well uniform with a size of about 2 μm. From Fig. 1I, MnS@MoS_2 microcubes show similar structure to $MnCO_3$ microcubes because MnS template is not removed so that MoS_2 can be intimate contact with MnS core. Therefore, MnS@MoS_2 microcubes are hard to identify. Nevertheless, from Fig. 1J, it shows that the shell with a large amount of exposed MoS_2 nanosheets, indicating MoS_2 nanosheets closely grow on MnS microcubes. As shown in Fig. 1K, a cubic void can be obviously viewed. Fig. 1L displays a large amount of MoS_2 nanosheets composing the microcubes. As shown in the inset of Fig. 1M, the microcube shell is with a thickness of about 400 nm. In virtue of the hollow structure and the ultrathin nanosheets, the as-prepared MoS_2 microboxes possess relatively large Brunauer–Emmett–Teller (BET) surface areas of 51.2 $m^2 g^{-1}$ (Fig. 1N).

The XRD patterns of $MnCO_3$, MnS@MoS_2 and MoS_2 microcubes are shown in Fig. 2A and 2B. All diffraction peaks of $MnCO_3$ are faultlessly shown (JCPDS No. 07-0268) without detectable impurities (Fig. 2A). From Fig. 2B, the diffraction of MnS@MoS_2 shows the typical peaks at 15.6°, 27.5°, 33.1°, 34.3°, 49.3°, 56.4°, 61.8°, 73.6°, and 83.7°, which corresponds to (002), (111), (100), (200), (220), (110), (222), (400) and (331) planes of MoS_2 (JCPDS No. 37-1492) and MnS (JCPDS No.

72-1534), respectively. Three broad diffraction peaks center at about 15.6°, 33.1° and 56.4°corresponding to MoS_2 (JCPDS No. 37-1492) are observed.

Further insights of the structural of products were obtained from Raman spectrum (Fig. 2C and 2D). As shown in Fig. 2C, there are no other miscellaneous peaks, confirming that the products are pure phase. Fig. 2D shows broad peaks of MnS@MoS_2 observed at 267 cm^{-1} and 304 cm^{-1} are in accord with the transverse optical phonon and longitudinal optical phonon modes of vibrations, respectively. A resonance peak at 684 cm^{-1} is a photoluminescence band as earlier noted (Anastassiadou et al., 1989). In addition, both MoS_2 and MnS@MoS_2 exhibit characteristic E2g and A_{1g} Raman modes locating at 357 cm^{-1} and 409 cm^{-1}, respectively, indicating the presence of MnS and MoS_2 in MnS@MoS_2 microcubes.

3.3. Electrochemical characterization

CV was used to characterize different modified electrodes (Fig. 3). As shown in Fig. 3A, bare GCE displays a couple of redox peaks in 10 mM $[Fe(CN)_6]^{3-/4-}$ (curve a). Peak currents slightly decrease when hollow MoS_2 microcubes are applied on GCE due to semiconductor characters (curve b). AuNPs modified GCE (curve c) obviously increases peak current, indicating AuNPs can accelerate electron transfer. The current respond further enhances when AuNPs and MoS_2 microcubes are jointly modified on GCE (curve d). In addition, as shown in Fig. 3B, current responses decrease greatly when DNA capture probe is applied on electrode due to its hydrophobicity (curve e). The redox currents gradually decrease after electrode reacting with MCH and BSA (curves f, g) step by step due to the fact that protein and negative charges of DNA insulate conductive support and electron transfer becomes difficult. However, the redox currents slightly increase when miRNAs and DSN mixed solution are applied on

electrode due to capture probe strands are cleaved by DSN leading to reduce negative charges of DNA (curves h). The redox currents greatly decrease after electrode reacted with SA-ALP. CV results suggest the successful construction of biosensor.

EIS is one important technique to explore the characteristic of surface-modified electrodes. In the impedance spectra, the increase in diameter of the semicircle indicates the enhancement in interfacial electron transfer resistance (R_{et}). Fig. 3C shows the characteristic EIS correspondence with gradually modification processes. Bare GCE displays a R_{et} value of about 246 Ω (curve a). When MoS_2 is assembled on GCE, R_{et} increases to 260 Ω (curve b). R_{et} greatly decreases after AuNPs are modified on GCE due to good electro-conductivity (curve c). After AuNPs and MoS_2 are modified on GCE, R_{et} greatly decreases and exhibits almost a line (curve d). As shown in Fig. 3D, R_{et} value obviously increases after DNA capture probe is applied on electrode due to hindering electron transfer (curve e). When MCH and BSA (curves f and g) are applied on electrode, R_{et} value obviously increases, which may originates from the protein and negative charges DNA sequences blocking electrode surface. Nevertheless, R_{et} value obviously increases when miRNA/DSN mixed solution is added because DSN can cleave capture probe strands (curves h). R_{et} value greatly decreases after SA-ALP is applied on electrode due to protein blocking electrode surface (curves i). The EIS results are consistent with CV.

Effective surface areas of GCE and AuNPs/MoS_2/GCE were compared by chronocoulumetry in 0.1 mM $K_3[Fe(CN)_6]$ solution containing 1.0 M KCl, where the standard diffusion coefficient (D_0) of $K_3[Fe(CN)_6]$ at 25 °C is 7.6×10^{-6} cm^2 s^{-1}. The effective surface area (A) of electrodes is calculated according to following equation:

$$Q = 2nFAcD^{1/2}t^{1/2}/\pi^{1/2} + Q_{dl} + Q_{ads} \quad (1)$$

where n is the number of electron transferred, F (C mol^{-1}) is Faraday constant, A (cm^2) is area of electrode, c (mol cm^{-3}) is concentration of substrate, D (cm^2 s^{-1}) is diffusion coefficient, Q_{dl} (C) is double layer charge and Q_{ads} (C) is adsorption charge and other symbols have their usual significances. According to results shown in Fig. 3E and 3F, A is calculated to be 0.016 cm^2 and 0.094 cm^2 for bare GCE and AuNPs/MoS_2/GCE, respectively. The results manifest that effective surface area of electrode increases significantly after modification with AuNPs/MoS_2 film.

Fig. 3G shows the signal-amplification effect of as-prepared material. Current signal greatly increases when MoS_2 is employed in sensor construction (curve b). The corresponding signal gain in the presence of MoS_2 microcubes is about 253.4% for that in the absence of MoS_2 microcubes (curve a), indicating MoS_2 microcubes are helpful to enhance detection sensitivity.

3.4. Optimization of experimental conditions

To obtain good analytical performance, several experimental conditions were optimized. The effect of deposition time of AuNPs was tested in range of 10–80 s (Fig. S1A). The highest current response is obtained at a deposition time of 40 s. So 40 s was used.

The working temperature of hybridization/DSN was used at 65 °C in accordance with a previous protocol (Liu et al., 2014). For purpose of attaining the highest sensitivity and low cost, DSN concentration and incubation time were tested. As shown in Fig. S1B, DPV response decreases with increase of DSN concentration, and then almost stays stable when it exceeds 0.01 U μg^{-1}. So, DSN concentration of 0.01 U μg^{-1} was employed in further experiments. As shown in Fig. S1C, DPV response decreases with incubation time increase, and then almost keeps stable when it exceeds

60 min, confirming that hybridization/degradation reaction mediated by DSN is almost accomplished within 60 min. Therefore, 60 min of incubation time was employed in the subsequent experiments.

3.5. Feasibility of detection system

In this work, detection system was based on SA-ALP catalysis of oxidation substrate of AAP, TCEP and FCM. Fig. 4A shows DPV responds of BSA/MCH/Capture DNA/AuNPs/MoS_2/GCE in different substrate solutions. It shows that no redox response is observed in solutions of AAP (curve a) and AAP/TCEP (curve b), indicating the insulating DNA/MCH self-assembled monolayers hinder electro-oxidation of AA. In FcM system, generated AA causes an obvious increase in the redox response of FcM (curve c). The electrode reaction is feature of an electrochemical–chemical (EC) reaction mechanism, indicating FcM mediates the electron transfer between AA and electrode. Moreover, the presence of TCEP induces a more significant increase in peak current (curve f). The peak current of AAP/TCEP/FcM is 13 times than that of only FcM, indicating AAP/TCEP/FcM system can greatly improve detection signal. This result is attributed to the regeneration of AA from its oxidized product by TCEP on account of TCEP itself unable trigger a variation in the redox response of FcM (curve d). All above indicate that EC reaction occurs between FcM and AA, the chemical–chemical (CC) reaction occurs between AA and TCEP, and the CC reaction are able to promote EC reaction. Thus, EEC redox cycling can greatly amplify electrochemical signal, which therefore leads to a low detection limit.

3.6. Sensitivity to target miRNA-21

The sensitivity for detecting miRNA-21 was demonstrated by DPV under the optimal conditions. Fig. 4B shows peak currents decrease with increasing miRNA concentration. For quantification, the current variation ΔI (ΔI = I − I_0, where I and I_0 represent the peak currents in the presence and absence of miRNAs, respectively) is used here to evaluate analytical merits. As can be seen in the inset of Fig. 4B, there is a good linear relationship between ΔI and the logarithm of the concentration of miRNA in range from 0.1 fM to 0.1 pM. Peak current values are obtained from the mean value with three independent experiments. The linear calibration equation is ΔI = 65.69 + 4.09 log (c/M) with correlation coefficient R of 0.997, and detection limit is 0.086 fM (S/N=3). The analytical performances of different assays are compared in Table 1. The proposed assay exhibits the lowest detection limit which is attributed to the selective cleavage of DNA-miRNA by DSN and dual signal amplification of MoS_2 microcubes and ECC redox cycling.

3.7. Selectivity

In order to validate the selectivity of proposed biosensor, different miRNA sequences were tested. As shown in Fig. 4C, higher ΔI is obtained with complementary sequence than other mismatched sequence and non-complementary sequence. The ΔIs of non-complementary sequence and three-based mismatch sequence are negligible, indicating both mismatched miRNAs do not hybridize with capture probe. For single-base mismatched sequence, ΔI is 3.36 μA and only 10.8% of that of complementary sequence. These results indicated good selectivity of proposed assay.

3.8. Real sample analysis

To evaluate the applicability of developed miRNA biosensor, five human serum samples of breast cancer patients (confirmed by pathological examinations) obtained from Xinyang Central Hospital (Xinyang, China) were tested. Signed informed consent was obtained from each patient participating in the study before surgery. All serum samples were heated at 95 °C for 10 min before use. As references, expression levels of the serum miRNA-21 were simultaneously quantified by a commercial qRT-PCR kit. The analytical results are shown in Table S1, which shows the results obtained with proposed biosensors are in good agreement with those obtained by qRT-PCR, confirming the practical value of developed biosensor.

4. Conclusions

We report a sensitive electrochemical sensor for miRNA-21 detection, which is fabricated based on hierarchical hollow MoS_2 microcubes coupling with miRNAs-initiated cleavage of DNA by DSN and signal amplification of enzyme. This strategy has several excellent features. Firstly, MoS_2 microcubes with large specific surface coupling with AuNPs act as an excellent sensing substrate. Secondly, DSN can cleave DNA-miRNAs duplexes and miRNAs strands can recycle in sample solution. Thirdly, the biosensor demonstrates high selectivity due to rigorous hybridization temperature and mismatch identification ability by the DSN. Finally, the application of signal amplification of enzyme couples with EEC redox cycling reaction lead to a remarkable low detection limit (0.086 fM). The simple operation procedure, high sensitivity and selectivity demonstrate that the proposed method might be valuable for quantitative detection of miRNA in clinical diagnostic and prognostic.

Acknowledgments

This work was supported by the National Natural Science Foundation of China (U1304214, 21475115), Program for University Innovative Research Team of Henan (15IRTSTHN001), Henan Provincial Science and technology innovation team (C20150026), Nanhu Scholars Program of XYNU, University Students Sustentation Fund of Xinyang Normal University (No. 2016-DXS-23) and Science and Technology Major Project of Henan province (141100310600).

References

Akanda, M.R., Aziz, M.A., Jo, K., Tamilavan, V., Hyun, M.H., Kim, S., Yang, H., 2011. Anal. Chem. 83, 3926–3933.

Anastassiadou, A., Liarokapis, E., Anastassakis, E., 1989. Solid State Commun. 69, 137–142.

Bi, S., Chen, M., Jia, X.Q., Dong, Y., 2015. Nanoscale 7, 3745-3753.

Chhowalla, M., Shin, H.S., Eda, G., Li, L.J., Loh, K.P., Zhang, H., 2013. Nat. Chem. 5, 263–275.

Degliangeli, F., Kshirsagar, P., Brunetti, V., Pompa, P.P., Fiammengo, R., 2014. J. Am. Chem. Soc. 136, 2264–2267.

Dong, H., Lei, J., Ding, L., Wen, Y., Ju, H., Zhang, X., 2013. Chem. Rev. 113, 6207–6233.

Fei, J. B., Cui, Y., Yan, X.H., Qi, W., Yang, Y., Wang, K.W., He, Q., Li, J.B., 2008. Adv. Mater. 20, 452–456.

Gao, W.Y., Wang, M.Q., Ran, C.X., Li, L., 2015. Chem. Commun. 51, 1709–1712.

Gao, Z., 2012. Analyst 137, 1674–1679.

Ge, Z.L., Lin, M.H., Wang, P., Pei, H., Yan, J., Shi, J.Y., Huang, Q., He, D.N., Fan, C.H., Zuo, X.L., 2014. Anal. Chem. 86, 2124−2130.

Guo, Y.W., He, M.W., Xu, J.L., Ding, Y.P., 2013. J. Xinyang Normal Univ., Nat. Sci. Ed. 2, 283–287.

Hong, C.Y., Chen, X., Liu, T., Li, J., Yang, H.H., Chen, J.H., Chen, G.N., 2013. Biosens. Bioelectron. 50, 132–136.

Huang, K.J., Liu, Y.J., Wang, H,B., Wang, Y.Y., Liu, Y.M., 2014a. Biosens. Bioelectron. 55, 195–202.

Huang, K.J., Zhang, J.Z., Liu, Y.J., Wang, L.L., 2014b. Sensor. Actuat. B. 194, 303–310.

Hunt, E.A., Broyles, D., Head, T., Deo, S.K., 2015. Annu. Rev. Anal. Chem. 8, 217–237.

Hwang, H., Kim, H., Cho, J., 2011. Nano Lett. 11, 4826–4830.

Leshkowitz, D., Horn-Saban, S., Parmet, Y., Feldmesser, E., 2013. RNA 19, 527−38.

Li, W., Jiang, W., Ding, Y.S., Wang, L., 2015. Biosens. Bioelectron. 71, 401–406.

Liu, L., Xia, N., Liu, H., Kang, X., Liu, X., Xue, C., He, X., 2014. Biosens. Bioelectron. 53, 399–405.

Liu, S.P., Su, W.Q., Li, Z.L., Ding, X.T., 2015. Biosens. Bioelectron. 71, 57–61.

Liu, Y., Zhu, M.Q., Chen, D., 2015. J. Mater. Chem. A. 3, 11857–11862.

Luo, D.F., Liu, X., 2015. J. Xinyang Norm. Univ., Nat. Sci. Ed., 28, 542-545.

Miao, P., Wang, B., Yu, Z., Zhao, J., Tang, Y., 2015. Biosens. Bioelectron. 63, 365–370.

Ou, J.Z., Chrimes, A.F., Wang, Y.C., Tang, S.Y., Strano, M.S., Kalantar-zadeh, K., 2014. Nano Lett. 14, 857–863.

Wang, H.B., Zhang, H.D., Xing, Z.H., Li, X.L., Chen, Y., 2015, J. Xinyang Norm. Univ., Nat. Sci. Ed., 28, 550-554.

Wang, M., Li, B.C., Zhou, Q., Yin, H.S., Zhou, Y.L., Ai S.Y., 2015. Electrochim. Acta. 165, 130–135.

Wang, X., Wang, W.M., Liu, Y., Ren, M.M., Xiao, H.N., Liu, X.Y., 2011. Anal. Chem. 83, 3926–3934.

Wen, Y., Liu, G., Pei, H., Li, L., Xu, Q., Liang, W., Li, Y., Xu, L., Ren, S., Fan, C., 2013. Methods 64, 276–282.

Xi, Q., Zhou, D.M., Kan, Y.Y., Ge, J., Wu, Z.K., Yu, R.Q., Jiang, J.H., 2014. Anal. Chem. 86, 1361–1365.

Xia, N., Zhang, Y.J., Wei, X., Huang, Y.P., Liu, L., 2015. Anal. Chim. Acta. 878, 95–101.

Yang, H., 2012. Curr. Opinion Chem. Biol. 16, 422-428.

Yang, L., Liu, C., Ren, W., Li, Z., 2012. ACS Appl. Mater. Interfaces. 4, 6450-6453.

Yin, H.S., Zhou, Y.L., Chen, C.X., Zhu, L.S., Ai, S.Y., 2012. Analyst 137, 1389–1395.

Zhang, L., Miranda-Castro, R., Stines-Chaumeil, C., Mano, N., Xu, G., Mavré, F., Limoges, B., 2014. Anal. Chem. 86, 2257–2267.

Zhu, C., Zeng, Z., Li, H., Li, F., Fan, C., Zhang, H., 2013. J. Am. Chem. Soc. 135, 5998–6001.

Table 1 Comparison between the proposed assay and other method for miRNA detection.

Electrodes	Analytical technique	Linear range (pM)	LOD (fM)	References
$Os(bpy)_2(API)Cl$-activated GO	Amperometric current–time curve	0.008–10	4	(Gao, 2012)
HRP/TMB/gold GCE	Amperometric current–time curve	0.01–1000	10	(Wen et al., 2013)
HRP/AuNPs/graphene	DPV	0.001–700	6	(Yin et al., 2012)
AuNPs/ALP/redox cycling	Amperometric current–time curve	0.001–5	3	(Liu et al., 2014)
QDs/RP/GODPS/GCE	fluorescence dots	0.05–1	5	(Li et al., 2015)
IgG-ALP/AuNPs/GCE	DPV	0.0005–0.5	0.4	(Wang et al., 2015b)
SA-ALPs/gold GCE	mperometric current–time curve	0.0005–1	0.2	(Xia et al., 2015)
AuNPs/MoS_2 /GCE	DPV	0.0001–100	0.086	This work

Figure captions

Scheme 1. Schematic illustration of the strategy for miRNA-21 detection based on AuNPs/MoS_2 modified electrode and using the signal amplification of duplex-specific nuclease and and ECC redox cycling.

Fig. 1. SEM images of $MnCO_3$ microcubes (A-B), MnS@MoS_2 microcubes (C, D) and MoS_2 microcubes (E, F), BSA/MCH/Capture DNA/AuNPs/MoS_2/GCE after reacted with miRNA/DSN (G); TEM images of $MnCO_3$ microcubes (H), MnS@MoS_2 microcubes (I, J) and MoS_2 microcubes (K-M); N_2 adsorption-desorption isotherm of the MoS_2 microcubes (N).

Fig. 2. XRD pattern of $MnCO_3$ (A), MnS@MoS_2 and MoS_2 microcubes (B); Raman spectra of $MnCO_3$ (C), MnS@MoS_2 and MoS_2 microcubes (D).

Fig. 3. CVs (A, B) and EIS (C, D) of bare GCE (a), MoS_2/GCE (b), AuNPs/GCE (c), AuNPs/MoS_2/GCE (d), Capture DNA/AuNPs/MoS_2/GCE (e), MCH/Capture DNA/AuNPs/MoS_2/GCE (f), BSA/MCH/Capture DNA/AuNPs/MoS_2/GCE (g), BSA/MCH/Capture DNA/AuNPs/MoS_2/GCE after reacted with miRNA/DSN (h), SA-ALP/BSA/MCH/Capture DNA/AuNPs/MoS_2/GCE (i); (E) Plot of Q-t curves of bare GCE (a) and AuNPs/MoS_2/GCE (b) in 0.1 mM $K_3[Fe(CN)_6]$ containing 1.0 M KCl; (F) plot of Q-$t^{1/2}$ curves on GCE (a) and AuNPs/MoS_2/GCE (b); (G) DPVs of SA-ALP/BSA/MCH/Capture DNA/AuNPs/GCE (a) and SA-ALP/BSA/MCH/Capture DNA/AuNPs/MoS_2/GCE (b) in 10 mM Tri buffer solution (8.0) containing 5 mM TCEP and 2 mM FCM.

Fig. 4. (A) DPVs curves of BSA/MCH/Capture DNA/AuNPs/MoS_2/GCE in different solutions: AAP (a); AAP/TCEP (b); FcM (c); TCEP/FcM (d); AAP/FcM (e); and AAP/TCEP/FcM (f); (B) DPV curves responding to different miRNA concentrations (from a to j): 0, 1.0×10^{-16}, 1.0×10^{-15}, 1.0×10^{-14}, 1.0×10^{-13}, 5.0×10^{-13}, 1.0×10^{-12}, 5.0×10^{-12}, 1.0×10^{-11}, 1.0×10^{-10} M, respectively. Inset: the relationship between the current variation ΔI and the negatively logarithm of the miRNA concentration; (C) The selectivity of the sensor hybridized to different miRNA sequences: miRNA(a), single-based mismatch sequence (b), three-based mismatch sequence (c), and non-complementary sequence (d).

Scheme 1

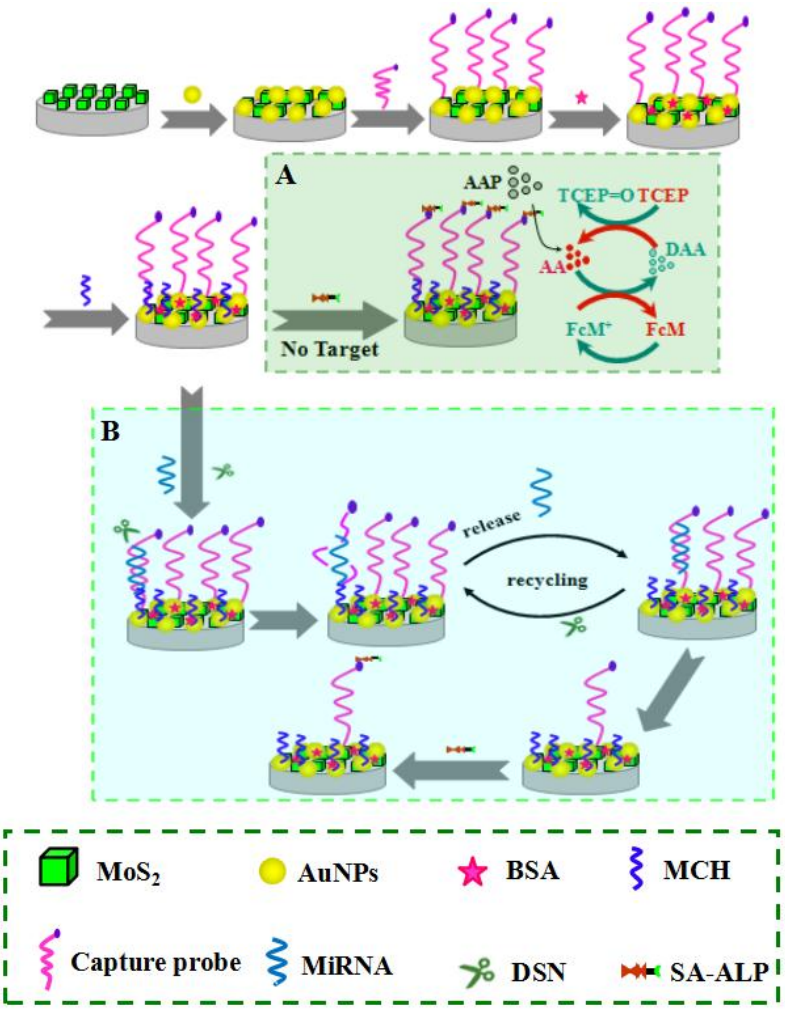

Figure 1

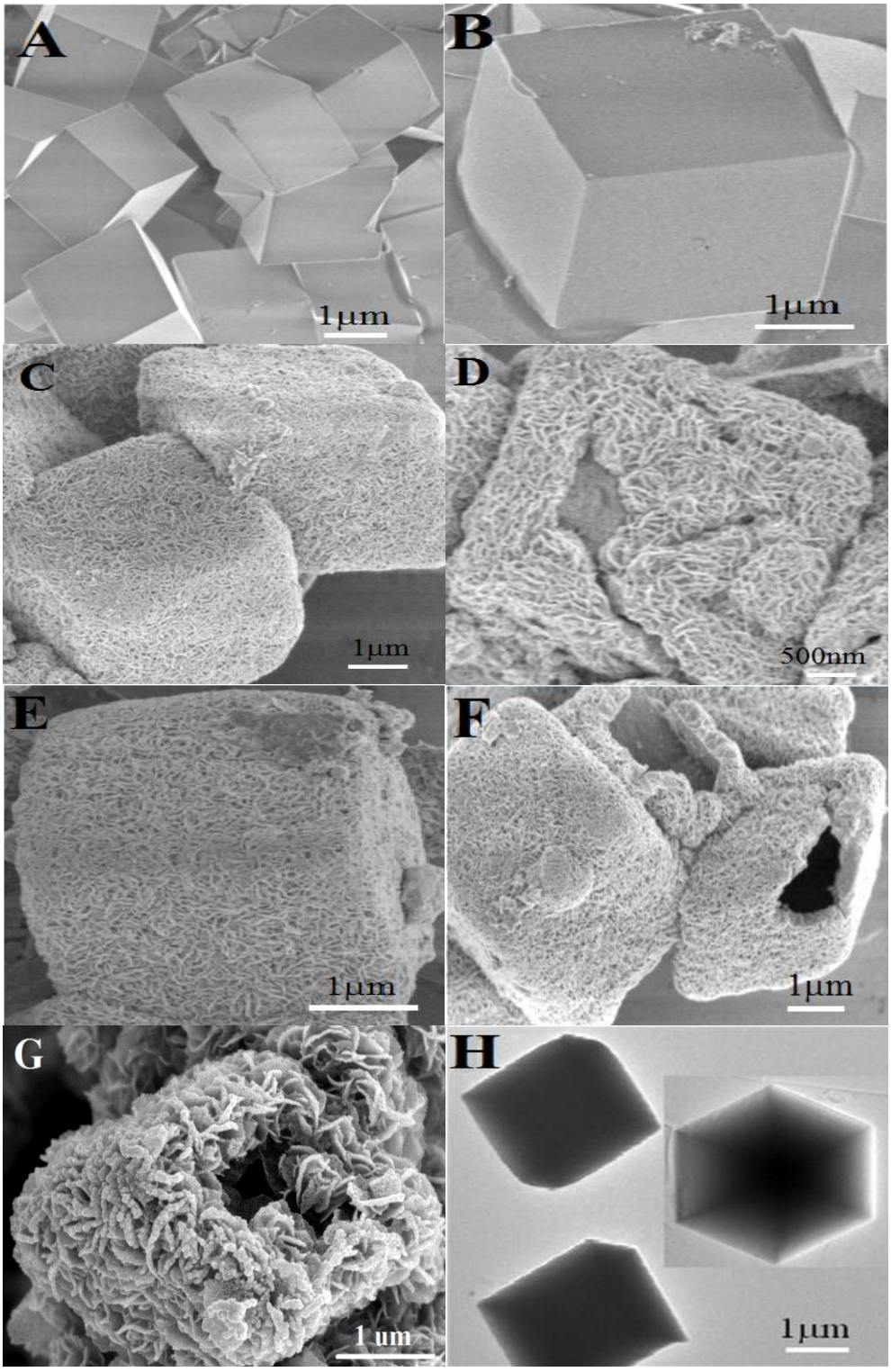

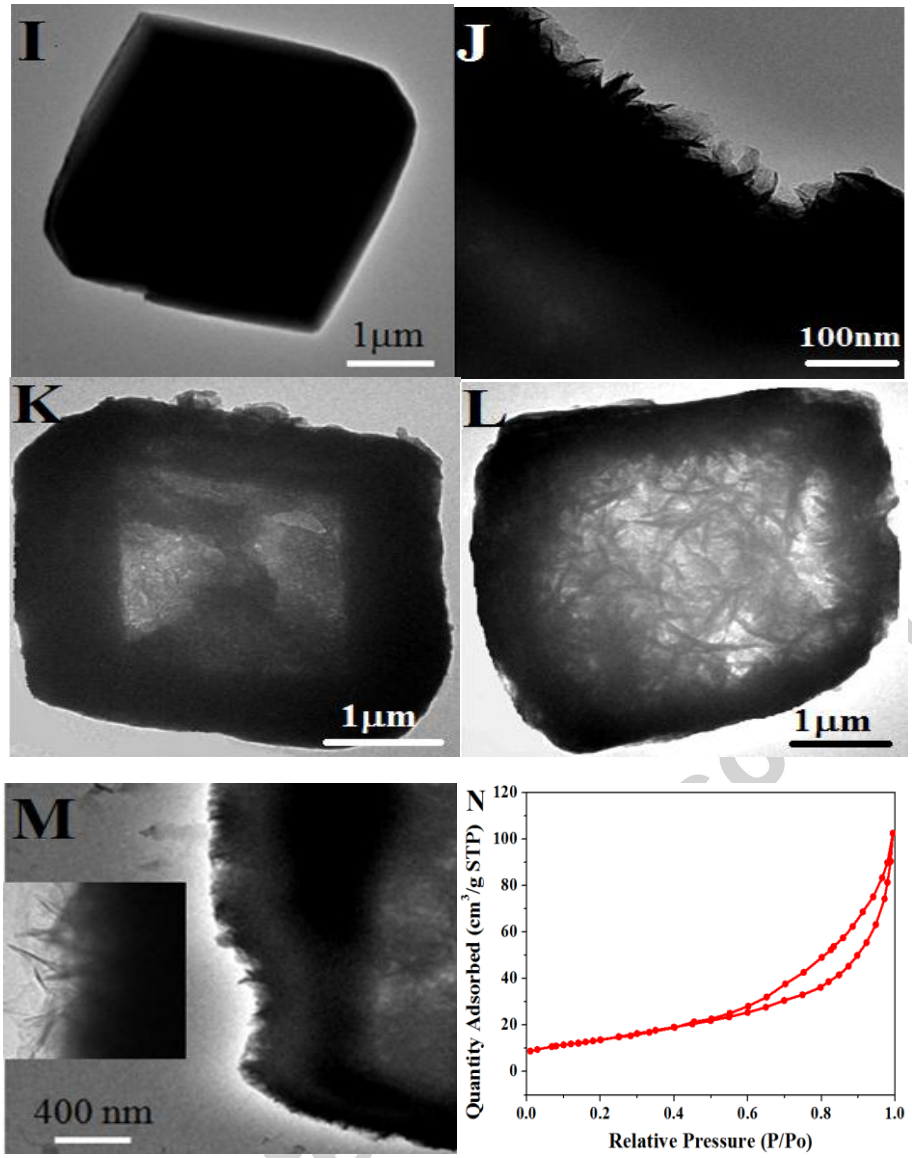
I
1μm
J
100nm
K
1μm
L
1μm
M
400 nm
N
Quantity Adsorbed (cm³/g STP)
Relative Pressure (P/Po)
0
20
40
60
80
100
120
0.0
0.2
0.4
0.6
0.8
1.0

Figure 2

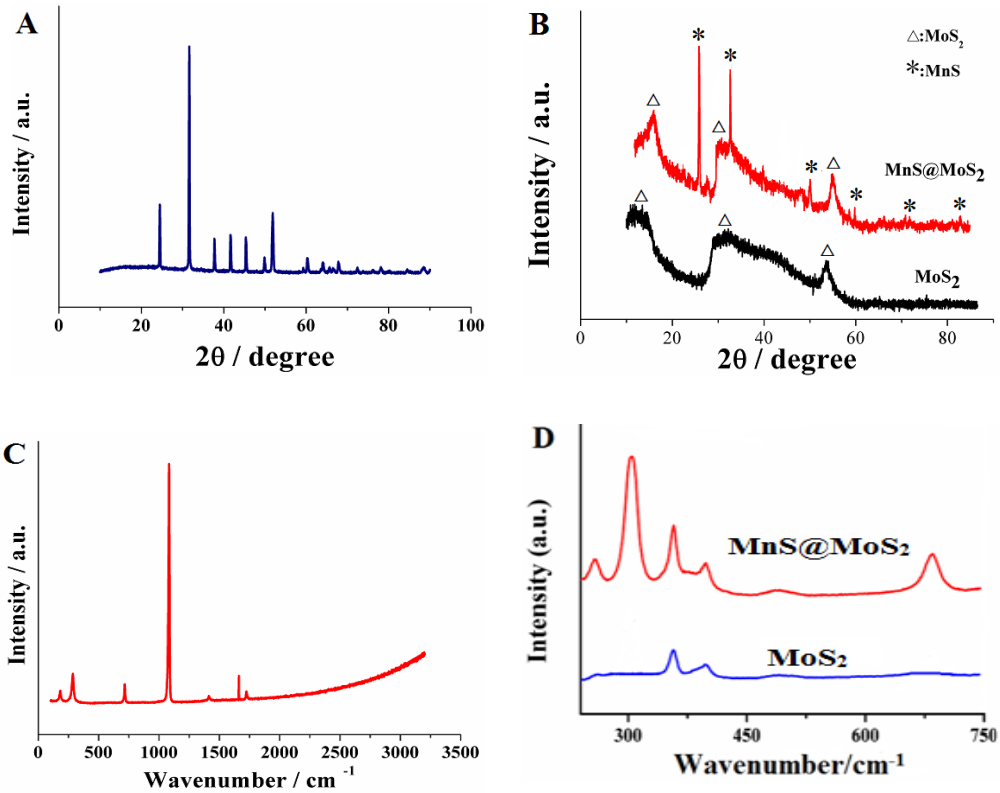

Figure 3

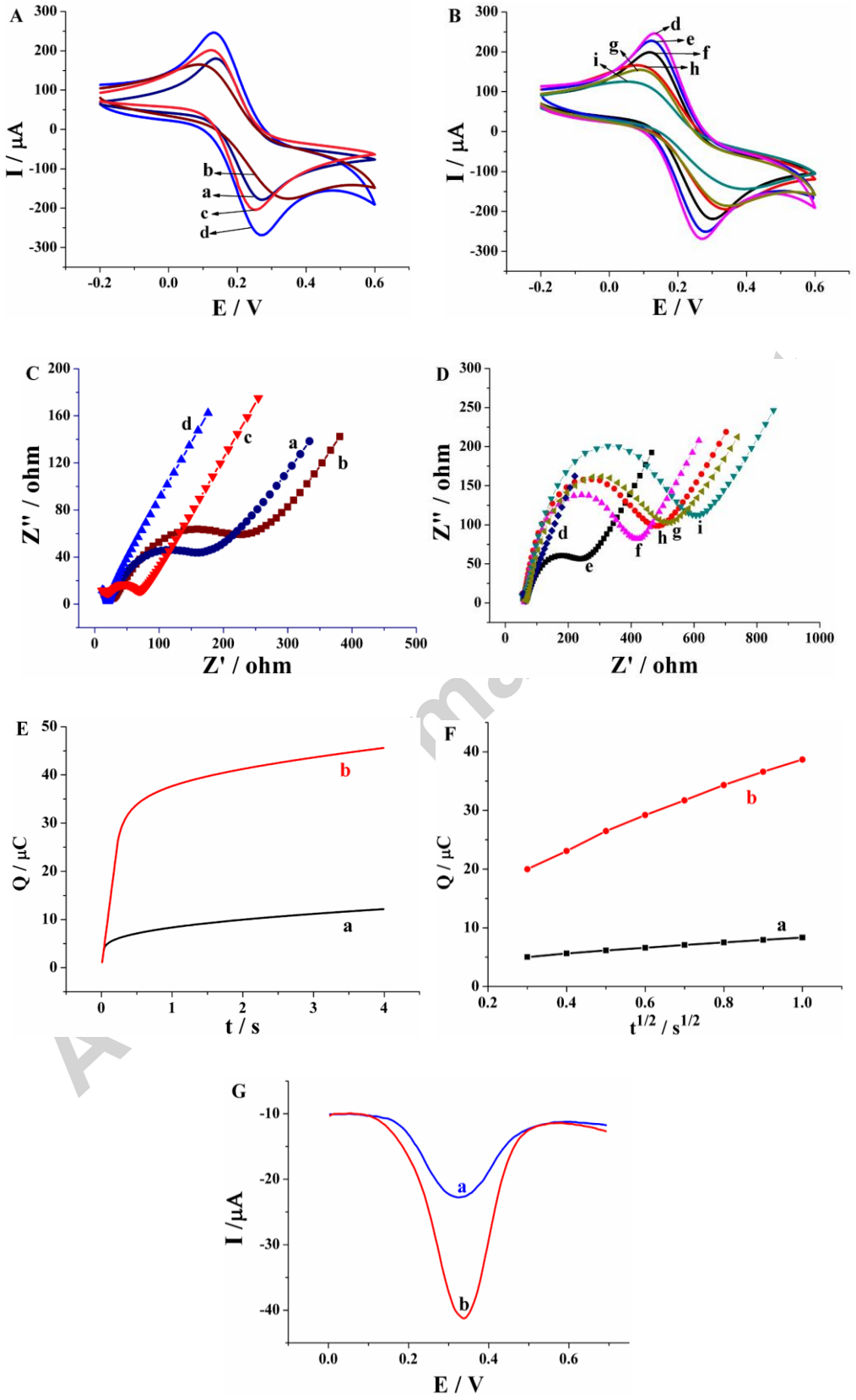
A
I / μA
E / V
b
a
c
d
B
I / μA
E / V
d
e
g
f
i
h
C
Z'' / ohm
Z' / ohm
d
c
a
b
D
Z'' / ohm
Z' / ohm
d
e
f
h
g
i
E
Q / μC
t / s
b
a
F
Q / μC
t^1/2 / s^1/2
b
a
G
I /μA
E / V
a
b

Figure 4

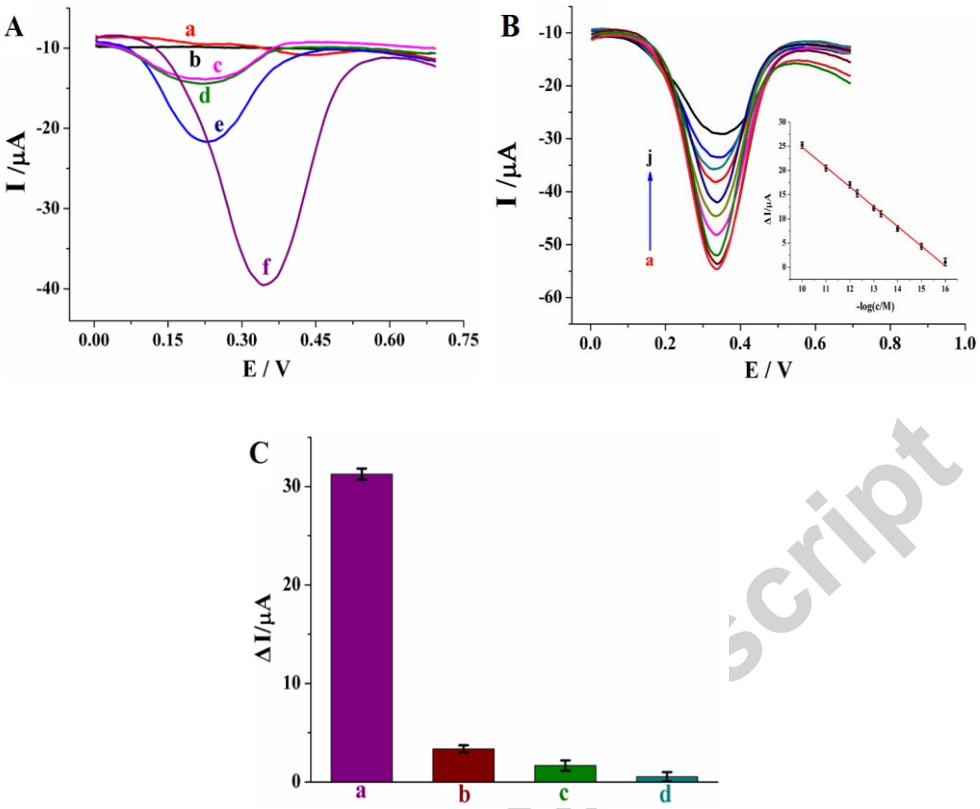

Highlights

- Facile hydrothermal method is used for the synthesis hollow molybdenum disulfide microcubes.
- A miRNA sensing platform is constructed based on duplex-specific nuclease and enzyme signal amplification.
- An electrochemical-chemical-chemical redox cycling system was used to amply detection signal.
- The biosensor shows a detection limit of 0.086 fM and high specificity towards target miRNA.